

Article

Au Nanoparticles Supported on Hydrotalcite-Based MMgAlO_x (M=Cu, Ni, and Co) Composite: Influence of Dopants on the Catalytic Activity for Semi-Hydrogenation of C₂H₂

Xun Sun ¹, Wenrui Lv ¹, Yanan Cheng ¹, Huijuan Su ¹, Libo Sun ¹, Lijun Zhao ¹ , Zifan Wang ^{2,3,*} and Caixia Qi ^{1,*}

- ¹ Shandong Applied Research Center of Gold Nanotechnology (Au-SDARC), School of Chemistry & Chemical Engineering, Yantai University, Yantai 264005, China; sunxun@ytu.edu.cn (X.S.); lwr03067719@ytu.edu.cn (W.L.); cyn17854111175@163.com (Y.C.); suhuijuan2012@ytu.edu.cn (H.S.); sunlibo@ytu.edu.cn (L.S.); zhaolijun0511@126.com (L.Z.)
- ² Key Laboratory of Biotechnology and Bioengineering of State Ethnic Affairs Commission, Biomedical Research Center, Northwest Minzu University, Lanzhou 730030, China
- ³ Engineering Research Center of Key Technology and Industrialization of Cell-Based Vaccine, Ministry of Education, Lanzhou 730030, China
- * Correspondence: zifanwang0316@gmail.com (Z.W.); qicx@ytu.edu.cn (C.Q.)

Abstract: Semi-hydrogenation of acetylene to ethylene over metal oxide-supported Au nanoparticles is an interesting topic. Here, a hydrotalcite-based MMgAlO_x (M=Cu, Ni, and Co) composite oxide was exploited by introducing different Cu, Ni, and Co dopants with unique properties, and then used as support to obtain Au/MMgAlO_x catalysts via a modified deposition–precipitation method. XRD, BET, ICP-OES, TEM, Raman, XPS, and TPD were employed to investigate their physic-chemical properties and catalytic performances for the semi-hydrogenation of acetylene to ethylene. Generally, the catalytic activity of the Cu-modified Au/CuMgAlO_x catalyst was higher than that of the other modified catalysts. The TOR for Au/CuMgAlO_x was 0.0598 h⁻¹, which was 30 times higher than that of Au/MgAl₂O₄. The SEM and XRD results showed no significant difference in structure or morphology after introducing the dopants. These dopants had an unfavorable effect on the Au particle size, as confirmed by the TEM studies. Accordingly, the effects on catalytic performance of the M dopant of the obtained Au/MMgAlO_x catalyst were improved. Results of Raman, NH₃-TPD, and CO₂-TPD confirmed that the Au/CuMgAlO_x catalyst had more basic sites, which is beneficial for less coking on the catalyst surface after the reaction. XPS analysis showed that gold nanoparticles exhibited a partially oxidized state at the edges and surfaces of CuMgAlO_x. Besides an increased proportion of basic sites on Au/CuMgAlO_x catalysts, the charge transfer from nanogold to the Cu-doped matrix support probably played a positive role in the selective hydrogenation of acetylene. The stability and deactivation of Au/CuMgAlO_x catalysts were also discussed and a possible reaction mechanism was proposed.

Keywords: nano-Au/MMgAlO_x catalysts; strong electronic interaction; semi-hydrogenation of C₂H₂; anti-coking



Citation: Sun, X.; Lv, W.; Cheng, Y.; Su, H.; Sun, L.; Zhao, L.; Wang, Z.; Qi, C. Au Nanoparticles Supported on Hydrotalcite-Based MMgAlO_x (M=Cu, Ni, and Co) Composite: Influence of Dopants on the Catalytic Activity for Semi-Hydrogenation of C₂H₂. *Catalysts* **2024**, *14*, 315. <https://doi.org/10.3390/catal14050315>

Academic Editor: Ana Paula da Costa Ribeiro

Received: 31 March 2024

Revised: 24 April 2024

Accepted: 7 May 2024

Published: 10 May 2024



Copyright: © 2024 by the authors. Licensee MDPI, Basel, Switzerland. This article is an open access article distributed under the terms and conditions of the Creative Commons Attribution (CC BY) license (<https://creativecommons.org/licenses/by/4.0/>).

1. Introduction

Selective hydrogenation of C₂H₂ is essential because petrochemicals involve many downstream products made from ethylene [1]. Small amounts of acetylene by-products from naphtha cracking to prepare ethylene exceed the 5 ppm limit for downstream products [2,3]. Semi-hydrogenation of acetylene to produce ethylene is recognized as the most efficient solution to this problem [4–8]. Therefore, developing a highly selective catalyst for acetylene hydrogenation is highly demanded [9].

Conventional palladium-based catalysts are commonly used due to their high efficiency in the ethylene conversion process [10]. The high costs of palladium-based cata-

lysts, their low selectivity for ethylene, and the formation of carbon deposits from over-hydrogenation products, which seriously affect the lifetime of the catalysts, are the main problems in current industrial applications [11–15]. Excessive hydrogenation of ethylene over palladium-based catalysts is due to the presence of consecutive palladium ensembles [16]. Researchers typically add a second metal to the catalyst to form disordered alloys or ordered metal structures to improve the catalytic performance of palladium-based catalysts [17–20]. Unfortunately, while this approach improves the selectivity of the palladium-based catalysts, the acetylene conversion decreases. This is due to the lower amount of palladium used in this method and the poor ability of isolated palladium atoms to activate H₂ [21–23]. Han's Pd@Ag/TiO₂ catalysts exhibited enhanced ethylene selectivity because the Ag shell layer blocks the high coordination sites on the palladium core [24]. Also, metal single-atom catalysts (SACs) exhibited approximately one-tenth the catalytic activity of nanoparticle catalysts [25]. In addition to this, the modification of supports has been heavily investigated [26,27]. Although previous methods improved ethylene selectivity, they had a negative impact on the catalytic activity of palladium-based catalysts. Therefore, developing new catalysts with high selectivity and stability is urgently needed.

Supported Au nanocatalysts have been extensively studied since the pioneering work of Haruta [28]. In addition to typical low-temperature CO oxidation, Au catalysts have shown great potential for various other reactions such as propylene epoxidation, glucose oxidation, acetylene hydrochlorination, and selective hydrogenation of nitroaromatics [29–33]. These studies have revealed that the Au nanocatalysts exhibit more significant potential than the palladium catalysts. Additionally, Au nanocatalysts are found to be considerably selective for ethylene in acetylene hydrogenation. This selectivity is attributed to the different desorption temperatures of C₂H₂ and olefins on the surface of Au nanoparticles [34–38]. Research has shown that smaller-sized Au particles have higher catalytic activity in hydrogenation. [35,39]. There is a debate about the active site of hydrogenation, with some researchers assuming that the metallic Au species are responsible, while others support the oxidized Au species as the active site [40–42]. The activation of H₂ usually limits the hydrogenation process. Studies suggest the H₂ activation site is at the interface between the Au and the support [43,44]. Therefore, the nature of the support is recognized as an essential factor affecting the catalytic activity of Au catalysts [45–48].

We conducted extensive research on Au catalysts that exhibit high selectivity towards ethylene. Y. Zhang et al. reported strong interactions between the N species on the support and Au nanoparticles, and the TOF value of Au/CNA was five times higher than that of Au/Al₂O₃ [49]. L. Sun et al. added CeO₂ to Au/Al₂O₃ catalysts to change the acid–base properties of the support surface and electronic states of the Au species to improve catalytic activity [50]. Also, they prepared Au/MgO_x–Al₂O₃ with different crystal structures ranging from mixed-phase to pure spinel. This opened promising possibilities for engineering the crystal phase of the support for highly efficient heterogeneous Au catalysts [51]. These studies have demonstrated that modification of the support is an effective means of improving catalyst activity [52]. All of the supporting studies mentioned above involved adding some dopants to the surface of the support through post-modification. In this work, we utilized the properties of hydrotalcite to prepare composite oxide supports by introducing dopants to study the effect of different M dopants (M=Cu, Ni, and Co) on Au/MMgAlO_x catalysts and their catalytic performance. X-ray diffraction (XRD), X-ray photoelectron spectroscopy (XPS), transmission electron microscopy (TEM), and temperature-programmed desorption (TPD) techniques were systematically used to characterize the catalysts. The catalytic performance of a fixed-bed microreactor for C₂H₂ semi-hydrogenation was investigated.

2. Results and Discussion

2.1. Characterization of the Catalysts

2.1.1. Crystal and Structural Properties

Figure 1 shows the results of the nitrogen adsorption–desorption isotherm to characterize the surface area and pore size of the obtained catalysts. All catalysts exhibited typical type IV nitrogen adsorption–desorption isotherms as shown in Figure 1a. In addition, hysteresis loops coinciding with the structure of the mesoporous material were observed between 0.4 and 1.0 relative pressure [50]. The pore size distribution of the Au/MgAl₂O₄, Au/NiMgAlO_x, and Au/CoMgAlO_x catalysts shown in Figure 1b was found to be relatively narrow, with an average pore size of about 4.0 nm. In contrast, the Au/CuMgAlO_x catalysts had a much broader pore size distribution, with an average pore size of approximately 11.0 nm. Table 1 summarizes the physical properties of each catalyst. The BET surface area of the Au/CuMgAlO_x and Au/CoMgAlO_x catalysts was found to be much higher than that of the Au/MgAl₂O₄ catalyst. Among all, Au/CuMgAlO_x had the highest BET surface area of 233 m² g^{−1}. In contrast, Au/NiMgAlO_x had a significantly lower BET surface area of 69 m² g^{−1}. As shown in Table 1, the pore volumes of the Au/MgAl₂O₄ and Au/NiMgAlO_x catalysts were relatively small: 0.21 and 0.13 cm³ g^{−1}, respectively. However, the Au/CuMgAlO_x catalyst had a larger pore volume of 0.85 cm³ g^{−1}. These results indicate that doping with Cu and Co improved the catalysts' pore structure, which led to an increase in both the specific surface area and pore volume.

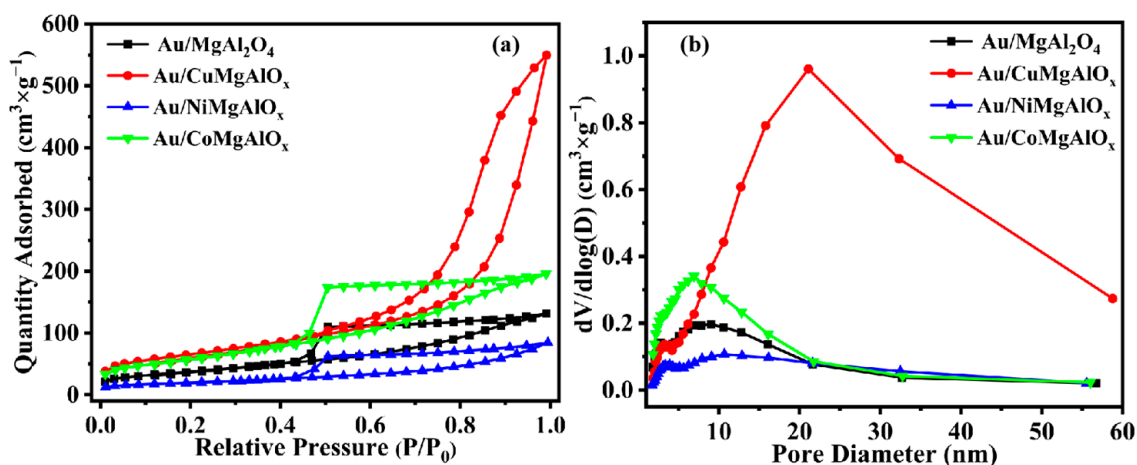


Figure 1. (a) Nitrogen adsorption and desorption isotherms; and (b) pore size distribution of catalysts.

Table 1. BET surface area and porous property of the studied catalysts.

Catalyst	$S_{\text{BET}}/\text{m}^2 \text{g}^{-1}$	$D_{\text{pore}}/\text{nm}$	$V_{\text{pore}}/\text{cm}^3 \text{g}^{-1}$
Au/MgAl ₂ O ₄	136	4.1	0.21
Au/CuMgAlO _x	233	11.0	0.85
Au/NiMgAlO _x	69	4.3	0.13
Au/CoMgAlO _x	212	3.9	0.31

XRD characterized the crystal structure of the Au/MMgAlO_x catalysts. As shown in Figure 2a, the characteristic diffraction peaks at 2θ values of 11.9°, 60.9°, and 66.1° correspond to the crystalline planes of hydroxalcite flakes (003), (113), and (116) (JCPDS 35-0964). This indicates that the lamellar structure of the hydroxalcite in the catalysts remained intact and was not destroyed [53]. The diffraction peaks related to the (311) and (400) crystal planes of the MgAl₂O₄ phase (JCPDS 21-1152) were observed at 36.9° and 45.1° for each catalyst. These peaks indicate that the layered structure of the hydroxalcite precursor partially transformed into the MgAl₂O₄ structure after calcination and reduction [54]. As shown in Figure 2b, the characteristic diffraction peak of the MMgAlO_x (M=Cu, Co)

support prepared by thermal decomposition tends to disappear at 11.9° , indicating a high degree of decomposition of the Mg-Al hydrotalcite, which may be the reason for its larger specific surface area. However, after loading gold, the crystallinity of the (003) plane of the Mg-Al hydrotalcite increases significantly. The relatively low ratio of Al: Mg (mol: mol) in the catalyst preparation raw materials, approximately 1:1 (mol:mol), results in partial substitution of Mg^{2+} by Al^{3+} in the hydrotalcite framework, leading to the formation of Al-O-Al. This could be one of the reasons why the samples retain a partial hydrotalcite structure even after a high-temperature treatment at $500^\circ C$ [55]. On the other hand, the alkaline treatment process for preparing the gold catalyst may trigger the “memory effect” of the hydrotalcite, transforming some metal oxides into the Mg-Al hydrotalcite structure [53]. No diffraction peak related to CuO, NiO, and CoO was observed in the XRD, which suggests that CuO, NiO, and CoO were well dispersed in the catalyst bulk phase [56]. Similarly, Au was well dispersed in the catalyst.

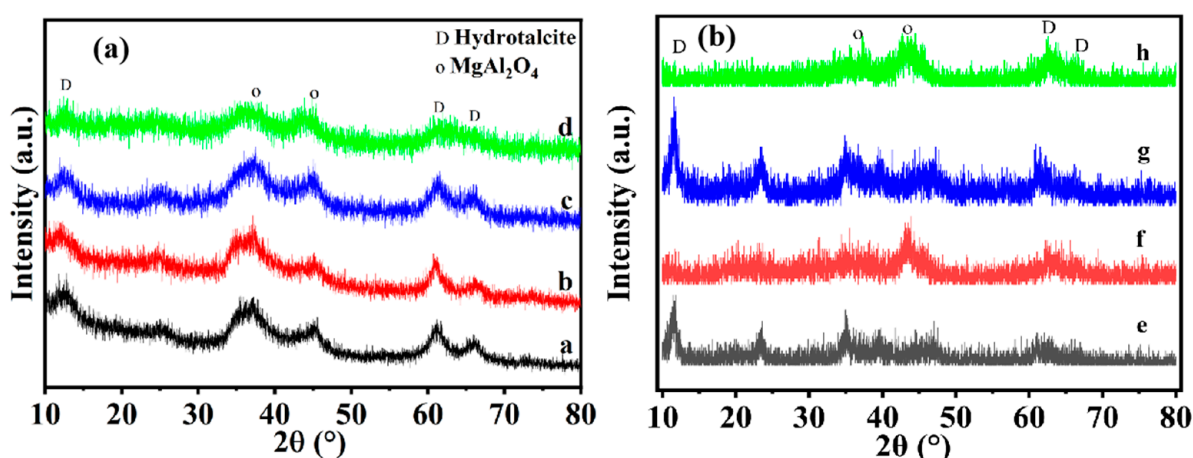


Figure 2. XRD patterns of Au/MgAl₂O₄ and Au/MMgAlO_x (M=Cu/Ni/Co) catalysts. (a: Au/MgAl₂O₄, b: Au/CuMgAlO_x, c: Au/NiMgAlO_x, d: Au/CoMgAlO_x, e: MgAl₂O₄, f: CuMgAlO_x, g: Au/NiMgAlO_x, and h: CoMgAlO_x).

The results of the ICP-OES analysis are listed in Table 2. The content of metal elements in the catalysts was similar to the dose used in the preparation process, which indicates that the dopant was successfully introduced into the hydrotalcite precursor.

Table 2. Element composition of bulk phase in catalysts.

Catalyst	Ingredient Ratio (mol)			Physical Composition (mol)		
	M	Mg	Al	M	Mg	Al
Au/MgAl ₂ O ₄	—	45	50	—	47.5	52.4
Au/CuMgAlO _x	5	45	50	5.3	47.4	47.2
Au/NiMgAlO _x	5	45	50	5.7	47.6	46.6
Au/CoMgAlO _x	5	45	50	5.1	47.5	47.3

2.1.2. Catalyst Morphology and Particle Size Distribution of Au Nanoparticles

SEM and HRTEM images of the Au/MMgAlO_x series catalysts are displayed in Figure 3. The SEM images (Figure 3a,c,e,g) all showed a hydroaluminat lamellar structure in morphology. It was found that there was no significant difference in morphology between catalysts doped with different metals and undoped catalysts.

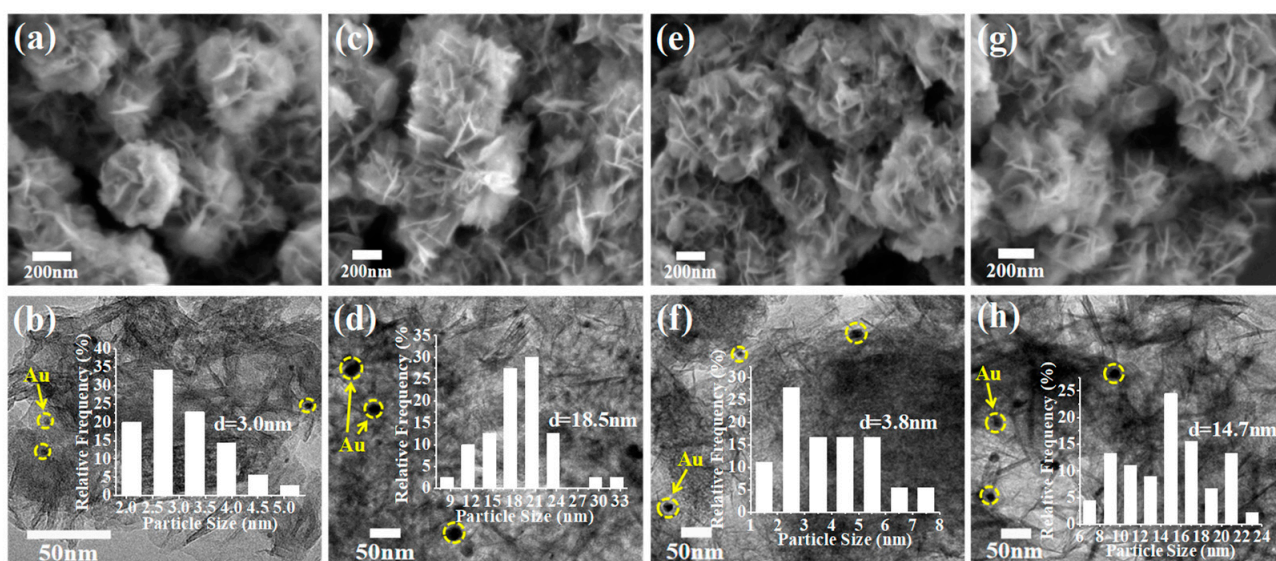


Figure 3. SEM and HRTEM images and particle size distribution of catalysts. (a,b) Au/MgAl₂O₄, (c,d) Au/CuMgAlO_x, (e,f) Au/NiMgAlO_x, and (g,h) Au/CoMgAlO_x.

Numerous studies have shown that the particle size of Au has an important effect on the performance of catalysts. In general, the smaller the Au particle size of the nano-Au catalyst, the higher its catalytic activity [35,39,57]. HRTEM images of each catalyst and the size distribution of Au particles are shown in Figure 3b,d,f,h. The Au nanoparticles for all four catalysts were spherical and uniformly dispersed on the support. Among them, the sizes of the Au nanoparticles of the Au/MgAl₂O₄ and Au/NiMgAlO_x catalysts were smaller, with average particle sizes of 3.0 and 3.8 nm, respectively. In contrast, Au particle sizes of the Au/CuMgAlO_x and Au/CoMgAlO_x catalysts were larger, with average sizes of 18.5 nm and 14.7 nm, respectively. At lower pH values, Au NPs tend to increase in size through agglomeration and growth, while at higher pH values, they tend to decrease in size only through surface growth [58]. During the gold loading process, the transformation of metal oxides to a Mg–Al hydrotalcite structure in the Au/MMgAlO_x (M=Cu, Co) catalyst consumes a certain amount of OH[−]. This may be the reason for the larger particle size of its Au NPs. Interestingly, as described below, the Au/CuMgAlO_x catalyst with larger Au nanoparticles showed the highest catalytic activity at 250 °C compared to the other catalysts. Therefore, catalyst performance in this experiment is less affected by the size of the Au nanoparticles.

2.1.3. Acid–Base Property

The property of the acid–base is one of the influencing factors of catalyst performance, and characterization of the acid–base of the modified catalysts was carried out [59,60]. CO₂-TPD determined the alkalinity of different catalysts with CO₂ as the probe molecule. Figure 4a shows that all four catalysts exhibited CO₂ desorption peaks around 100 °C and 380 °C. Among them, the desorption peak at around 100 °C was of low intensity due to weak primary sites on the catalyst surface, corresponding to CO₂ adsorbed on the –OH groups on the surface. The more substantial desorption peak around 380 °C is due to the medium to robust primary site on the catalyst, corresponding to the adsorption of CO₂ by the M–O[−] in the catalyst [61]. The Au/CuMgAlO_x catalyst had the highest CO₂ desorption peak temperature of 390 °C. The temperatures of the carbon dioxide desorption peaks of the other catalysts were almost identical at 375 °C (Au/MgAl₂O₄), 374 °C (Au/NiMgAlO_x), and 373 °C (Au/CoMgAlO_x). Figure 4b represents the amount of CO₂ desorption calculated from the CO₂ desorption curve (at 380 °C), which reflects the amount of alkaline site on the catalyst's surface. The Au/MgAl₂O₄ catalyst had the lowest amount of CO₂ desorption at 2.97 mmol g^{−1}. The CO₂ desorption amounts of Au/NiMgAlO_x and Au/CoMgAlO_x

were 3.90 mmol g^{-1} and 3.84 mmol g^{-1} , respectively. The Au/CuMgAlO_x catalyst had the highest CO₂ desorption amount of 5.57 mmol g^{-1} , indicating that the amount of alkaline site on the surface of the Au/CuMgAlO_x catalyst was higher compared with the other catalysts. The above results show that some dopants (Ni and Co) had little effect on the fundamental strength of the catalyst surface but increased the base content of the catalyst. However, the fundamental strength of the catalyst was significantly increased, and the alkali content increased, with the introduction of the Cu species. The significant increase in the alkaline sites of the Au/CuMgAlO_x catalyst may be related to its larger specific surface area and excellent pore properties. In contrast, the relatively low crystallization degree of the Au/CoMgAlO_x catalyst may account for its lower increase in alkaline site content.

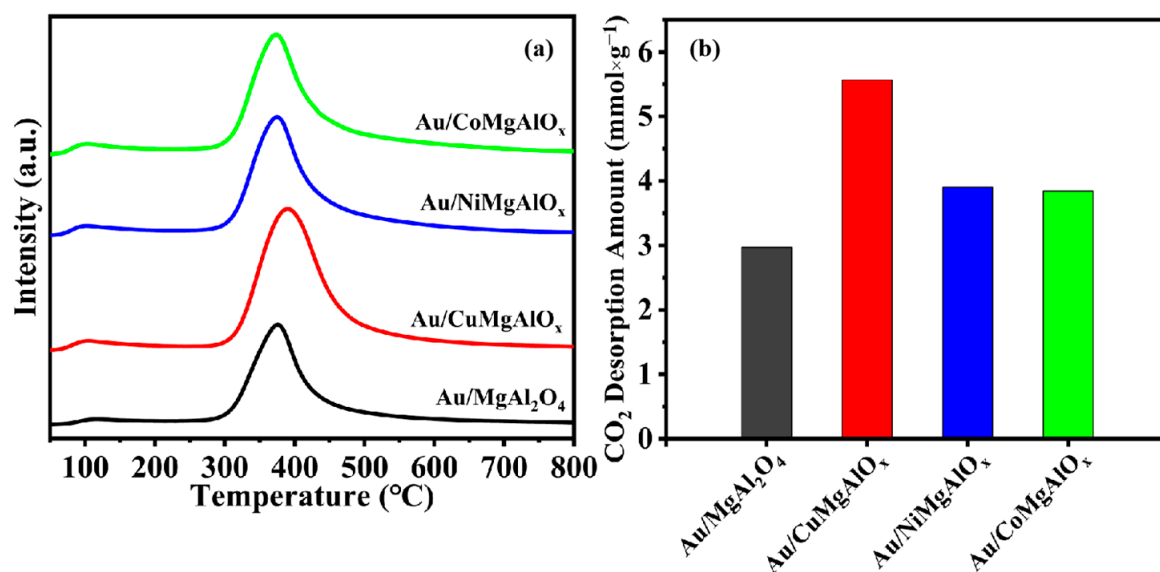


Figure 4. (a) CO₂-TPD curves; and (b) CO₂ desorption amount of Au/MgAl₂O₄ and Au/MMgAlO_x (M=Cu/Ni/Co) catalysts.

Subsequently, the acidity of the catalyst surface was investigated, using NH₃ molecules as probes, and the results are shown in Figure 5. Each catalyst had two peaks of NH₃ desorption: a weaker peak at around 110 °C and a more substantial peak at around 375 °C. The broad peak at 110 °C is attributed to the desorption from the weak acidic sites on the catalyst surface or physically adsorbed NH₃. The strong peak near 375 °C is attributed to the medium–strong acidic site on the catalyst surface due to the adsorption of NH₃ on the Lewis acidic site on the catalyst, according to previous reports [62]. The temperatures of the NH₃ desorption peaks did not differ much: they were 378 °C (Au/MgAl₂O₄), 380 °C (Au/CuMgAlO_x), 372 °C (Au/NiMgAlO_x), and 371 °C (Au/CoMgAlO_x), suggesting that the doping with different metals did not have much effect on the acidity of the catalyst surface. Based on the NH₃ desorption curve, the NH₃ desorption amount was calculated to compare each catalyst's acidic site on the surface. The amount of NH₃ desorption of Au/MgAl₂O₄ was the highest at 4.91 mmol g^{-1} , followed by Au/CuMgAlO_x at 3.76 mmol g^{-1} . The Au/NiMgAlO_x and Au/CoMgAlO_x catalysts had similar desorption amounts of around 3.0 mmol g^{-1} , which suggests that doping with metal reduces the amount of acid on the surface of the catalysts. According to reports, the Lewis acidic sites of Mg–Al mixed oxides are usually caused by Al³⁺ in the Al³⁺–O²⁻–Mg²⁺ structure. The possible introduction of metal oxides covers the Lewis acidic sites, resulting in the weakening of the Lewis acidity of Mg–Al mixed oxides [63].

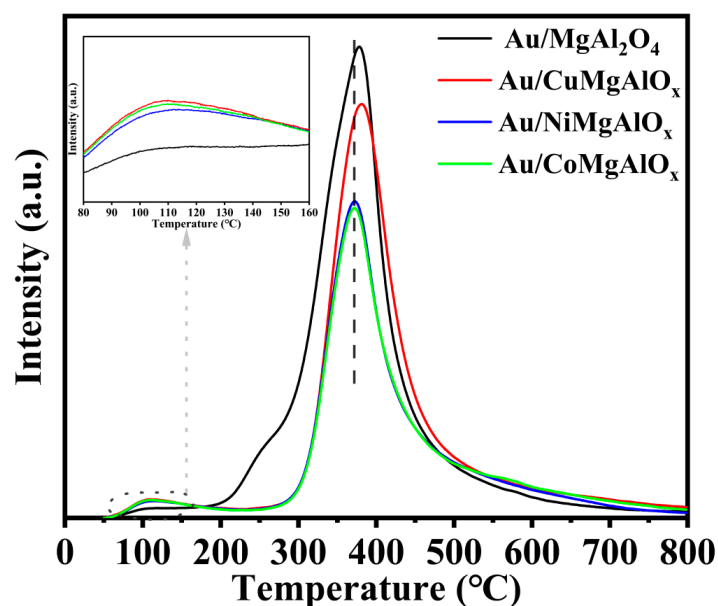


Figure 5. NH_3 -TPD curves of $\text{Au}/\text{MgAl}_2\text{O}_4$ and $\text{Au}/\text{MMgAlO}_x$ ($M=\text{Cu}/\text{Ni}/\text{Co}$) catalysts.

The base amount, acid amount, and base amount/acid amount data for each catalyst are summarized in Table 3. As shown in Table 3, $\text{Au}/\text{MgAl}_2\text{O}_4$ has the smallest base/acid amount of 0.60, $\text{Au}/\text{CuMgAlO}_x$ has the most significant base/acid amount of 1.48, and $\text{Au}/\text{NiMgAlO}_x$ and $\text{Au}/\text{CoMgAlO}_x$ have base/acid amounts of 1.32 and 1.29, respectively. X. Sun et al. have previously reported that, since acetylene belongs to the acidic molecules, the alkaline nature of the catalyst surface has a positive effect on the adsorption of acetylene on the Au surface, which can lead to a better catalytic performance of the catalyst [49]. Therefore, it was hypothesized that a higher base/acid ratio has an auxiliary effect on the adsorption of acetylene at the perimeter of Au nanoparticles, which is a potential reason for the higher acetylene conversion of the $\text{Au}/\text{CuMgAlO}_x$ catalyst.

Table 3. Acid and base amount of $\text{Au}/\text{MgAl}_2\text{O}_4$ catalyst and $\text{Au}/\text{MMgAlO}_x$ ($M=\text{Cu}/\text{Ni}/\text{Co}$) catalysts.

Catalyst	Base/ mmol g^{-1}	Acid/ mmol g^{-1}	Base/Acid
$\text{Au}/\text{MgAl}_2\text{O}_4$	2.97	4.91	0.60
$\text{Au}/\text{CuMgAlO}_x$	5.57	3.76	1.48
$\text{Au}/\text{NiMgAlO}_x$	3.90	2.96	1.32
$\text{Au}/\text{CoMgAlO}_x$	3.84	2.97	1.29

2.1.4. Chemical States of Au, Co, and Cu in Catalysts

The XPS for Au 4f of each catalyst is shown in Figure 6. A strong peak around 89 eV in the spectrum is due to the overlap of the binding energies of Mg 2s (89.0 eV) and Au 4f_{5/2} [64,65]. Therefore, the binding energy of Au 4f_{7/2} ($\text{Au}^0 = 84.0$ eV) was focused on. For the $\text{Au}/\text{MgAl}_2\text{O}_4$ catalyst with a smaller average Au particle size (3.0 nm), the peak at 84.1 eV indicates that the state of the gold on its surface should be the Au^0 species [66,67]. The surface of the $\text{Au}/\text{NiMgAlO}_x$ catalyst exhibits smaller Au NPs, and the characteristic peak of its Au 4f_{7/2} is observed at 84.3 eV. The binding energy of Au 4f is affected by the final state effect, and the larger Au particle size in some samples can influence its binding energy [68]. The binding energies of Au 4f_{7/2} for the $\text{Au}/\text{CoMgAlO}_x$ and $\text{Au}/\text{CuMgAlO}_x$ catalysts are 83.8 and 84.6 eV, respectively. The decrease in binding energy of Au 4f_{7/2} for the $\text{Au}/\text{CoMgAlO}_x$ catalyst may be related to the final state effect, while the positive shift in binding energy of Au 4f_{7/2} for the $\text{Au}/\text{CuMgAlO}_x$ catalyst with a larger average Au particle size may be attributed to the strong electronic interaction between Au and Cu species in the catalyst. On the XPS curve, a shift towards higher binding energy is generally

associated with a decrease in electron density or an increase in the oxidation state [69]. Therefore, we speculate that some Au on the surface of the Au/CuMgAlO_x catalyst is in an electron-deficient state [70].

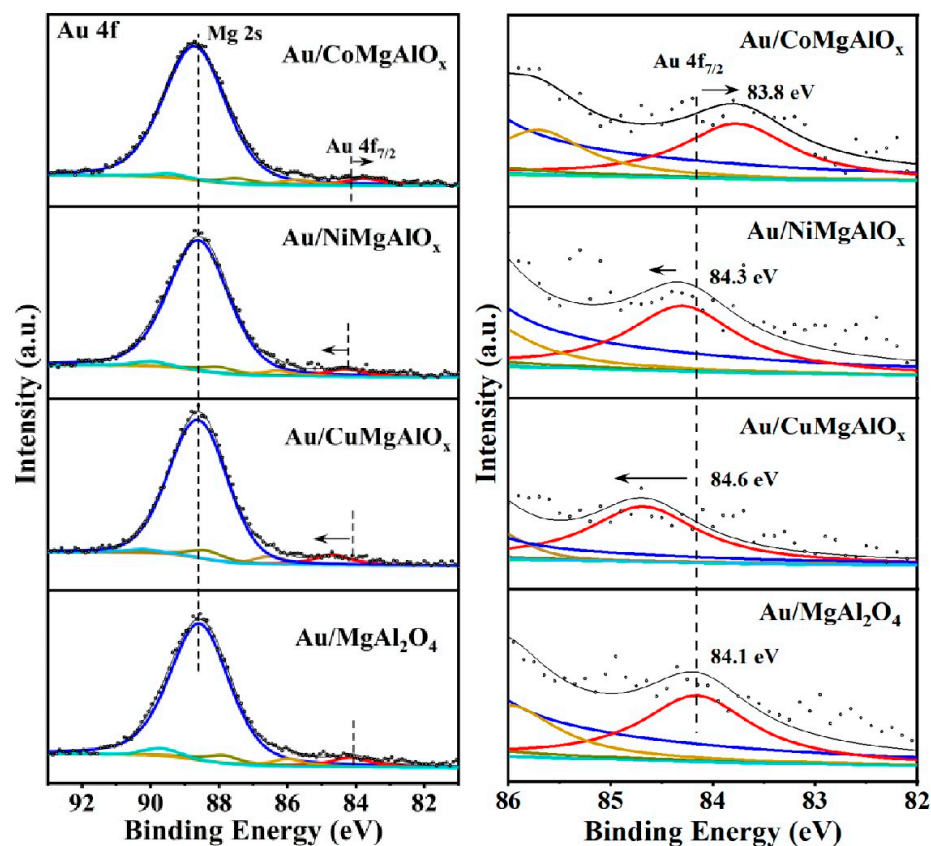


Figure 6. XPS profiles of Au 4f of Au/MgAl₂O₄ and Au/MMgAlO_x (M=Cu/Ni/Co) catalysts. (The right figure is the enlarged area of Au 4f_{7/2}).

As shown in Table 4, the concentration of heteroatoms (M=Cu, Co, and Ni) introduced on the surface of the Au/MMgAlO_x catalyst is significantly lower than that in the bulk phase. This suggests that the heteroatoms are not simply adsorbed on the surface of the catalyst, but rather form a composite oxide. The relatively high concentrations of C and O on the surface of the catalyst may be attributed to the Mg-Al hydrotalcite phase, which is consistent with the XRD results. The Au atoms are uniformly dispersed on the surface of the Au/MMgAlO_x catalyst. After introducing heteroatoms, the Mg/Al atomic ratio on the surface of the Au/CoMgAlO_x catalyst increases, which may be caused by the partial substitution of Mg²⁺ by Co²⁺. This observation is consistent with the results of the Co 2p XPS analysis. The decrease in the Mg/Al atomic ratio on the surface of the Au/CuMgAlO_x and Au/NiMgAlO_x catalysts compared to that of the Au/CoMgAlO_x catalyst may be related to the higher crystallization degree of the hydrotalcite phase.

Table 4. The surface atomic composition of the Au/MgAlO_x catalyst was determined through XPS analysis.

Catalyst	Atomic Content (%)					
	M	Au	Al	Mg	C	O
Au/MgAl ₂ O ₄	-	0.53	14.19	15.44	16.06	53.70
Au/CuMgAlO _x	0.75	0.41	16.57	13.34	15.19	53.10
Au/NiMgAlO _x	0.99	0.48	17.55	13.68	15.82	51.49
Au/CoMgAlO _x	0.64	0.50	13	15.46	16.48	52.53

In order to verify the electron transfer between Au and the supports, we analyzed the chemical valence states of Cu in Au/CuMgAlO_x and CuMgAlO_x, and the results are shown in Figure 7. As shown in Figure 7, Cu possibly exists in the catalyst in two forms. The appearance of satellite peaks at around 943.2 eV indicates the presence of Cu²⁺, but it is difficult to determine the presence of metallic Cu or Cu⁺ because both Cu¹⁺ and Cu⁰ contribute to the Cu 2p_{3/2} peaks [51]. In CuMgAlO_x, the characteristic peak of the Cu species is found near 934.4 eV, whereas the characteristic peak of the Cu²⁺ species in Au/CuMgAlO_x near 934.0 eV is shifted by 0.4 eV in the direction of low binding energy compared to CuMgAlO_x, indicating that the Cu²⁺ gained electrons [55]. Combined with the results of Au 4f spectroscopy, it was concluded that there was a strong electronic interaction between Au and Cu in the Au/CuMgAlO_x catalyst, and the electrons would be transferred from Au to Cu. L. Sun [50] et al. suggested that the positively charged Au (Au^{δ+}) promoted the adsorption of acetylene and the dissociation of H₂ in the selective hydrogenation reaction of acetylene.

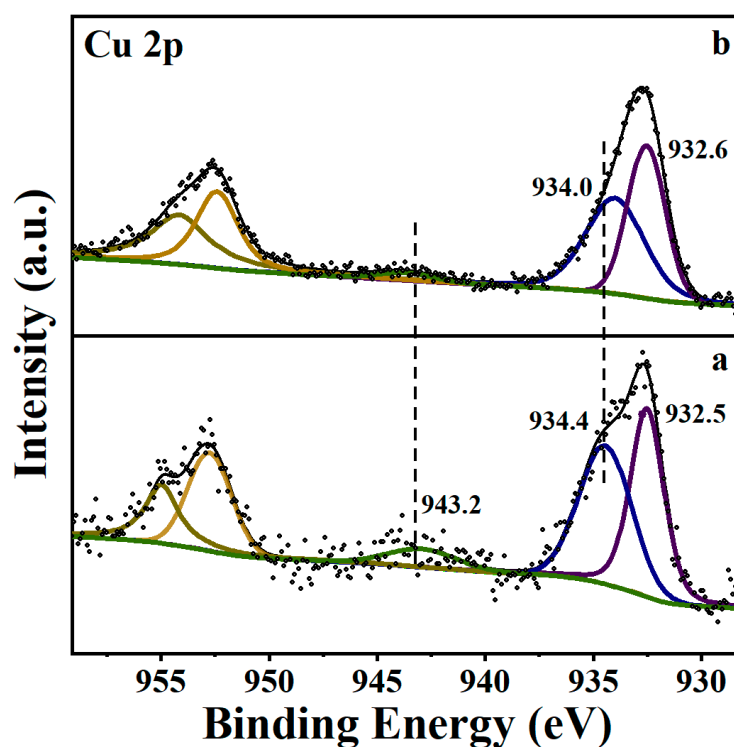


Figure 7. XPS profiles of Cu 2p of Au/CuMgAlO_x and CuMgAlO_x. (a) CuMgAlO_x; (b) Au/CuMgAlO_x.

As shown in Figure 8, the Co 2p spectrum consists of two satellite peaks (S₁ and S₂) and two sets of spin-orbit peaks, indicating the existence of two valence states of Co species on the catalyst surface. The characteristic peaks at 780.7 eV and 795.7 eV belong to Co³⁺, while the set of spin-orbit peaks with higher binding energy is attributed to Co²⁺ [71]. On the surface of the CoMgAlO_x sample, Co species mainly exist in the form of Co³⁺, while a large amount of Co²⁺ is found on the surface of the Au/CoMgAlO_x sample. This may be related to the reformation of the hydrotalcite phase. Through peak area integration, the area ratios of Co³⁺/Co²⁺ for the two catalysts are 2.55 (CoMgAlO_x) and 0.55 (Au/CoMgAlO_x), respectively. Therefore, we speculate that the decrease in the binding energy of the Au 4f_{7/2} orbit on the surface of the Au/CoMgAlO_x sample is mainly influenced by the final state effect.

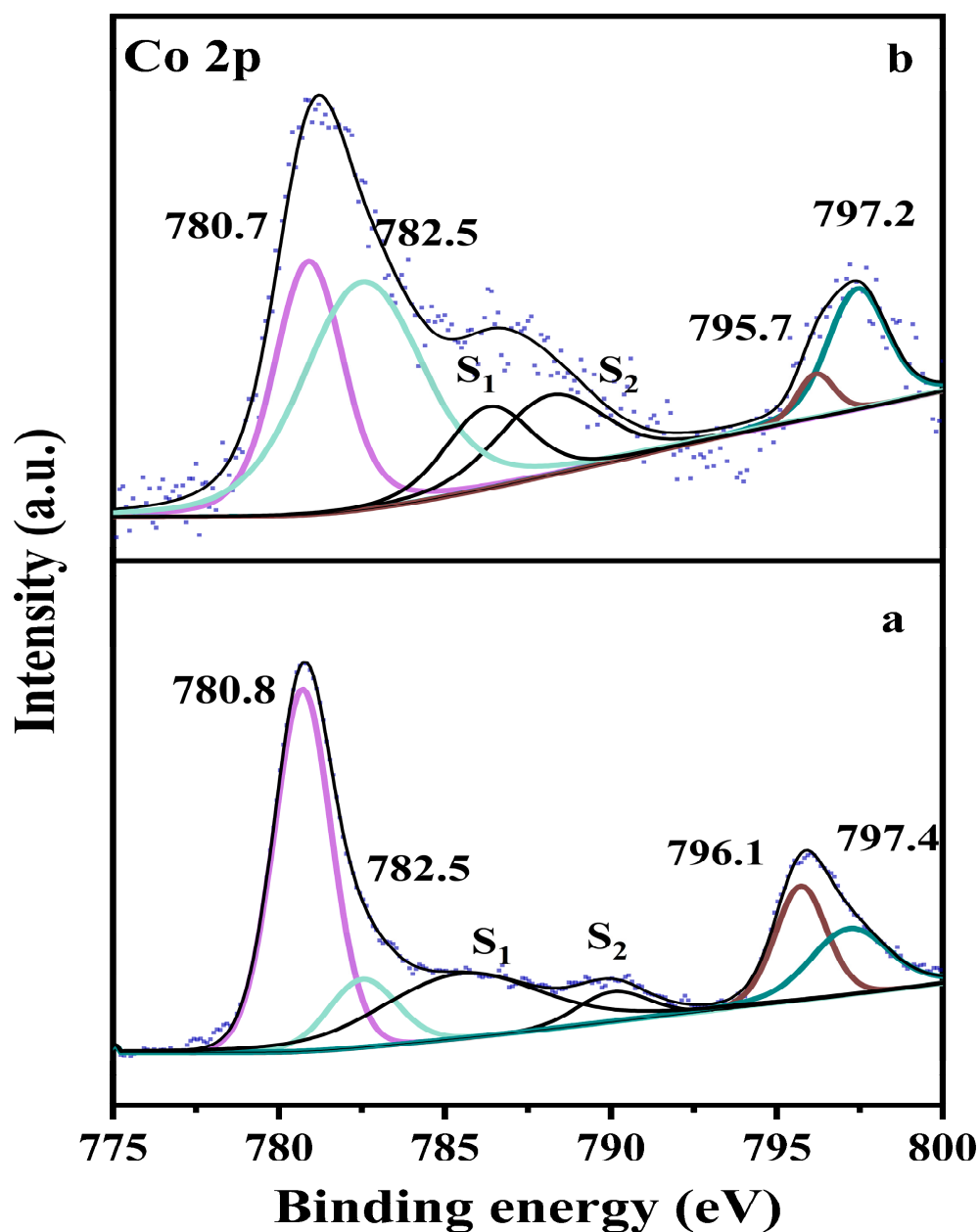


Figure 8. XPS profiles of Co 2p of Au/CoMgAlO_x and CoMgAlO_x. (a) CoMgAlO_x; (b) Au/CoMgAlO_x.

2.2. Catalytic Activity Tests

The catalytic performance of each catalyst in the acetylene selective hydrogenation reaction was tested, and the results are shown in Figure 9a. All catalysts showed catalytic activity above 150 °C. From the acetylene conversion curves in the figures, the acetylene conversions of Au/MgAl₂O₄ and Au/CoMgAlO_x catalysts increased slowly with the increase in reaction temperature, and the performance of the catalysts did not improve after doping with Co, but rather decreased. The acetylene conversions of Au/CuMgAlO_x and Au/NiMgAlO_x showed a trend of increasing up to 250 °C and then decreasing with the increase in the reaction temperature. At 250 °C the highest acetylene conversions of 32% for Au/CuMgAlO_x and 11% for Au/NiMgAlO_x were obtained, respectively. This phenomenon is consistent with the XPS results of Au 4f.

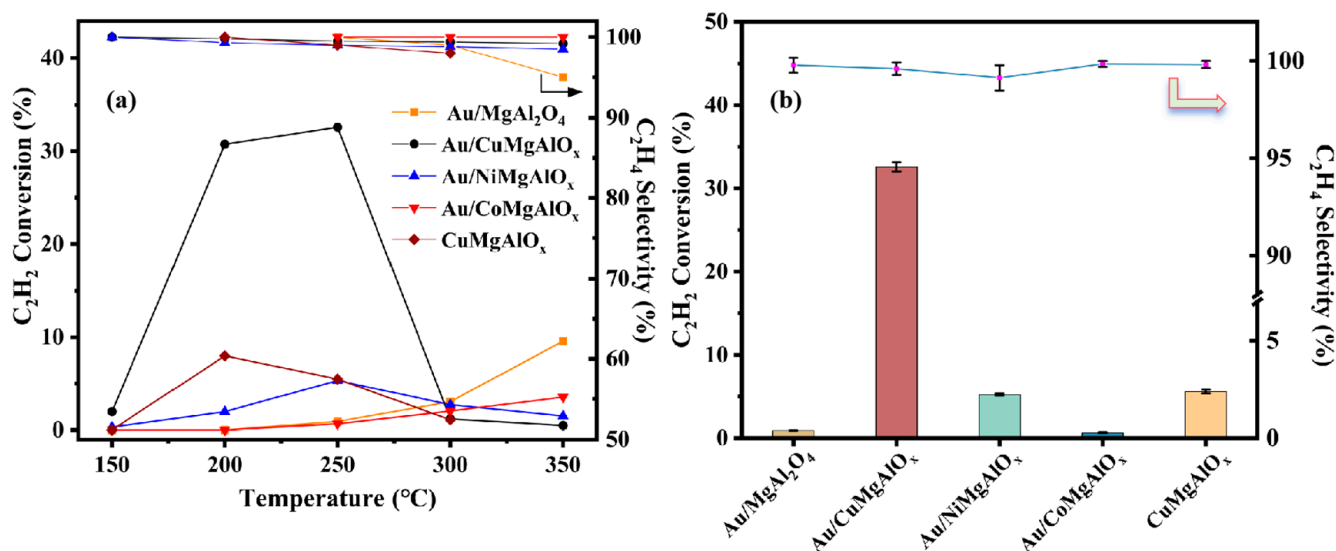


Figure 9. (a) Catalytic performance of catalysts; and (b) data error analysis (250 °C).

A comparison of the catalytic performance of the Au/CuMgAlO_x catalyst and its support CuMgAlO_x is also represented in Figure 9a. It can be seen that the acetylene conversion of CuMgAlO_x also tended to increase and then decrease as the reaction temperature increased, reaching a maximum value of 8% at 200 °C. CuMgAlO_x was rapidly deactivated at 250 °C, while Au/CuMgAlO_x achieved the highest acetylene conversion. Comparison of CuMgAlO_x and Au/CuMgAlO_x activity evaluation data reveals that the Au species play a crucial role in the C₂H₂ selective hydrogenation reaction. The conversion of Au/CuMgAlO_x is around four times higher than that of CuMgAlO_x while maintaining high selectivity. It was found that the performance of the catalyst was significantly improved after loading Au. The turnover rates (TORs) were calculated based on the total Au content and compared with the results of related studies. The TOR of Au/MgAl₂O₄ was only 0.016 h⁻¹ at 250 °C. However, the TOR value of Au/CuMgAlO_x was 0.059 h⁻¹. Its TOR was greater by a factor of about 37, while that of the Au/3%MgO_x-Al₂O₃-550 catalyst for the selective hydrogenation of C₂H₂ at 300 °C was 0.041 h⁻¹ [51]. This behavior can be plausibly explained by the exceptional physicochemical characteristics of the Au/CuMgAlO_x catalysts and the chemical valence states of the Au and Cu species on the surface. Overall, Au/CuMgAlO_x had a higher TOR at 250 °C, which implies that Au/CuMgAlO_x is a potential catalyst for C₂H₂ selective hydrogenation.

2.3. Coke Analysis and Stability

The stability of a catalyst is an important indicator for evaluating its performance. The time flow analysis of the two catalysts in the selective hydrogenation of acetylene at 200 °C under typical reaction conditions is shown in Figure 10. The initial activities of both catalysts agreed with the catalytic experiments' results. As shown in Figure 10, the Au/CuMgAlO_x catalyst decreased from an initial conversion of 30% to 24% in the first 420 min. Then, the Au/MgAl₂O₄ catalyst without dopant was deactivated after 180 min, followed by 500 min of a slow decay period. In summary, the catalytic performance of the Au/CuMgAlO_x catalyst was relatively stable. With the Cu introduction, the Au-based catalyst's initial activity reached 7 times that before modification, and compared to the Au/MgAl₂O₄, the catalytic activity was sustained for 2.3 times longer. Although the catalytic performance of the Au catalysts improved, the catalytic activity of the catalysts needs to be discussed in more detail in our subsequent work, especially in practical applications.

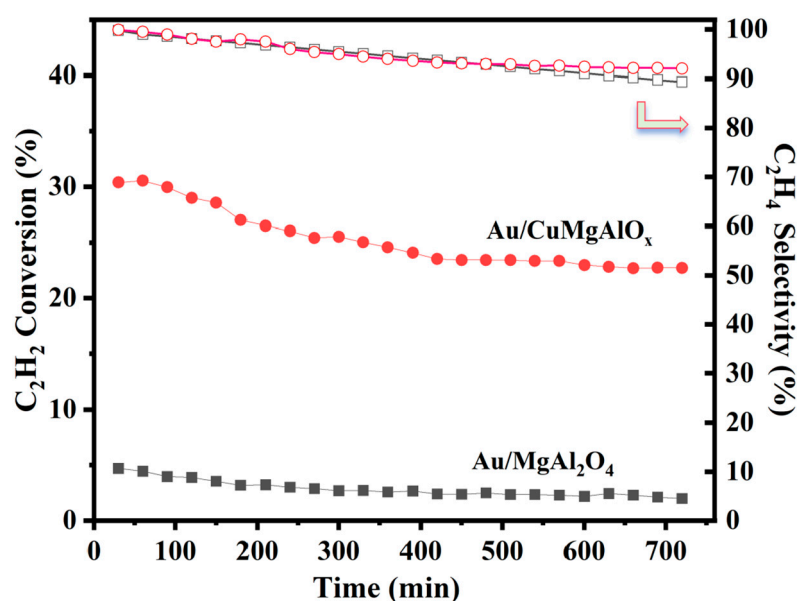


Figure 10. Evolution of acetylene conversion comparing the $Au/CuMgAlO_x$ to the $Au/MgAl_2O_4$ catalysts during the hydrogenation of acetylene at 200 °C.

In the acetylene selective hydrogenation reaction, its by-products (“green oil”) can quickly form carbonaceous deposits on the active metal surface of the catalyst, and the carbon buildup is an essential reason for the reduction in catalyst activity [72]. Raman spectroscopy is a powerful technique for detecting carbonaceous deposits on catalyst surfaces. Therefore, we performed Raman spectroscopic characterization of two catalysts after stability testing. As shown in Figure 11, the characteristic peaks near 1112 cm^{-1} and 1501 cm^{-1} of the $Au/MgAl_2O_4$ catalyst are attributed to the C species with amorphous and ordered or graphitic carbon structures, respectively, which suggests that the “green oil” produced on the surface of the $Au/MgAl_2O_4$ catalyst was partially converted to carbonaceous deposits during the stability test [50,51,73]. Therefore, we assume that the coverage of active sites on the surface of the $Au/MgAl_2O_4$ catalyst by carbonaceous deposits is an essential reason for its rapid deactivation in the stability test.

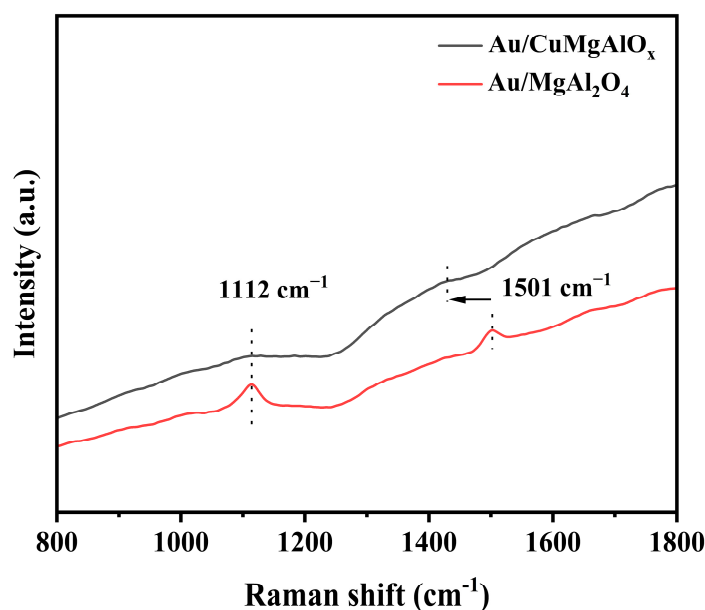


Figure 11. Raman spectra of the used $Au/CuMgAlO_x$ and $Au/MgAl_2O_4$ catalysts (after 12 h continuous hydrogenation reaction; gas condition: 0.6 vol% C_2H_2 /3.0 vol% H_2 /balance Ar).

However, the characteristic peaks of the Au/CuMgAlO_x catalyst near 1112 cm⁻¹ were significantly weaker in intensity, with a flattened peak shape and a broader peak top. Its characteristic peak near 1501 cm⁻¹ was displaced to 1420 cm⁻¹, and the peak intensity and shape were similar to those near 1112 cm⁻¹ [74]. This characteristic peak indicates the presence of a small amount of unsaturated aliphatic hydrocarbons on the catalyst surface instead of the ordered or graphitic carbon structure of the C species, which may be caused by the introduction of Cu species inducing a significant decrease in the percentage of acidic sites on the surface of the Au/CuMgAlO_x catalyst. The ordered or graphitic carbon structure is more inactive than the unstructured carbon, so we consider this an important reason for the better stability of the Au/CuMgAlO_x catalyst [74,75].

A comparison of TEM characterization and activity data revealed that Au particle size is not the main factor affecting the catalytic activity of Au/CuMgAlO_x and that oxidized Au species play an active role in the reaction. In order to investigate the main reason for the high-temperature deactivation of the catalyst, we analyzed the chemical valence states of the Au species on the catalyst surface after the high-temperature reaction by XPS. The Au 4f XPS patterns of the Au/CuMgAlO_x catalysts before and after the reaction are shown in Figure 12, and it can be clearly seen that the characteristic peaks of the Au species on the surface of Au/CuMgAlO_x were negatively displaced after the reaction. After the high-temperature reaction, the catalyst rapidly deactivated, and the Au species on its surface mainly existed in the metallic state. Therefore, we speculate that the strong electronic interaction between Au and Cu is the main reason for the high catalytic activity of the Au/CuMgAlO_x catalyst.

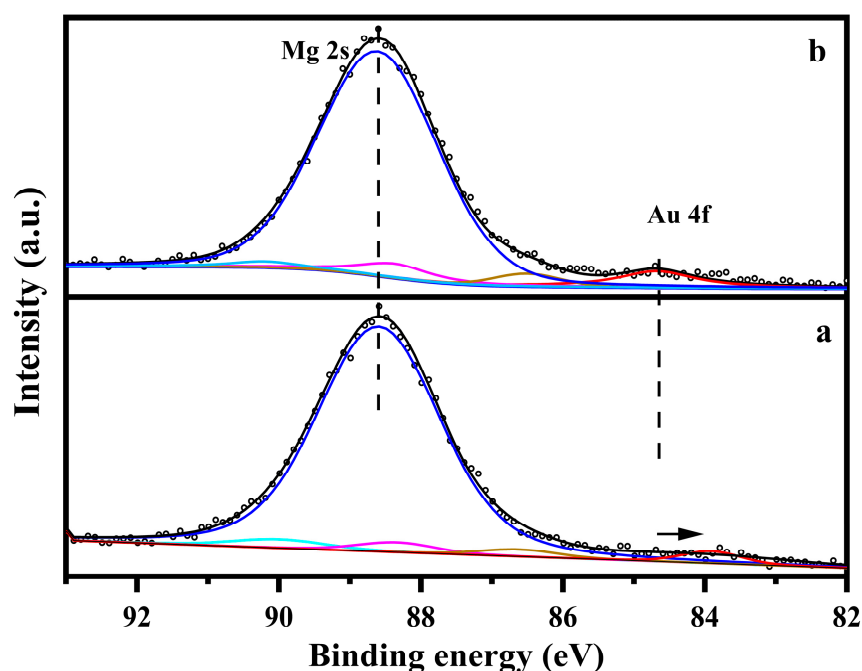


Figure 12. XPS profiles of Au 4f of Au/CuMgAlO_x. (a) Au/CuMgAlO_x-350; (b) Au/CuMgAlO_x.

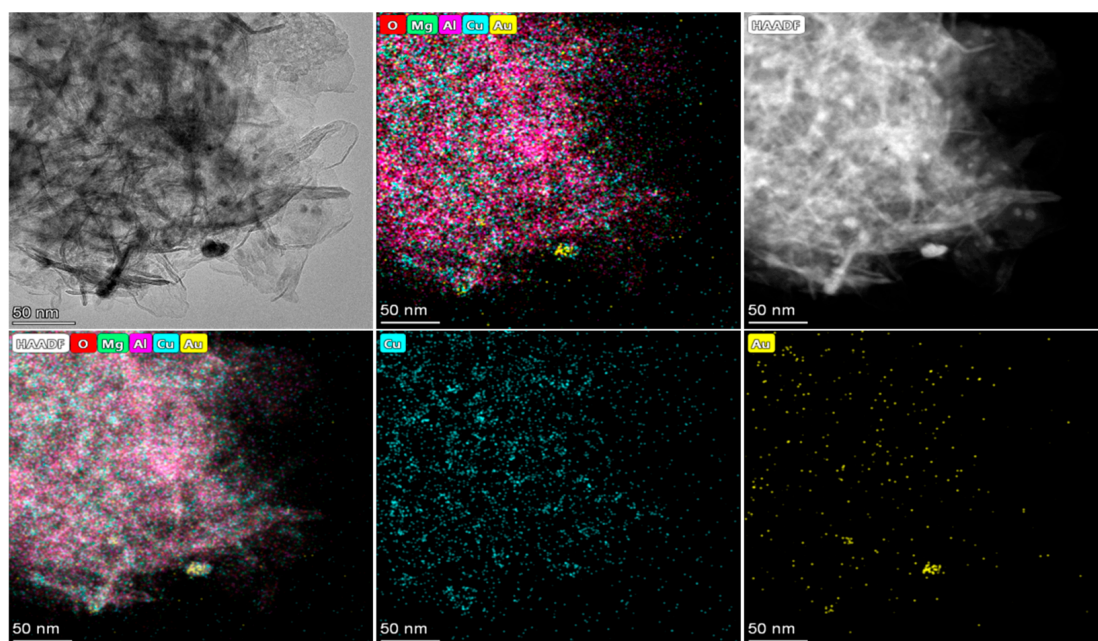
The surface atomic ratio of the samples after stability testing is shown in Table 5. The presence of a larger amount of C species on the catalyst's surface before the reaction may be caused by the incomplete decomposition of the hydrotalcite. After the reaction, no loss of Au species was observed for both catalysts. However, the surface C/Al ratio of the Au/MgAl₂O₄ catalyst increased from 1.13 to 2.12, while the surface C/Al ratio of the Au/CuMgAl₂O₄ catalyst only increased by 0.54. The Au/CuMgAlO_x catalyst exhibited better resistance to carbon deposition.

Table 5. Surface atomic ratio of the catalysts before and after the reaction determined by XPS analysis.

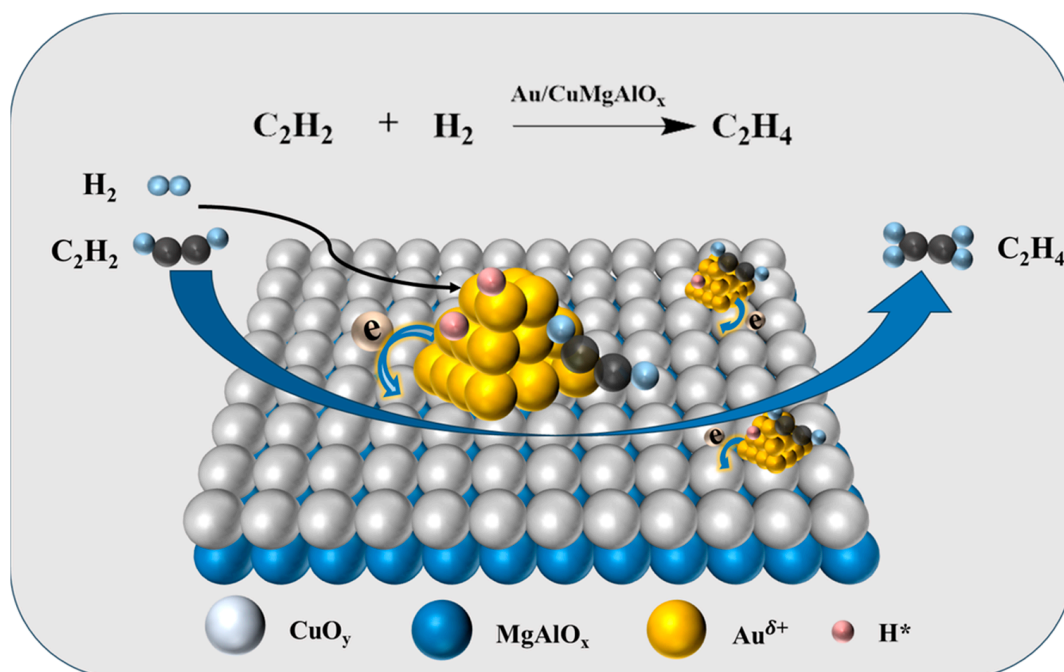
Catalyst	Atomic Ratio	
	Al/Au	C/Al
Au/MgAl ₂ O ₄	26.77	1.13
Au/CuMgAlO _x	40.41	0.92
Au/MgAlO _x -12 h	37.22	2.12
Au/CuMgAlO _x -12 h	27.31	1.46

2.4. Study on the Reduction Behavior of C₂H₂ on the Surface of the Au/CuMgAlO_x Catalyst

XPS analysis and activity data indicated that the electronic synergy between Au and copper is more favorable to the catalytic activity of the catalyst. Therefore, we performed TEM and EDS (HAADF) tests on the catalyst surface to study the elemental distribution on the catalyst surface. As shown in Figure 13, the Cu and Au species are uniformly distributed on the surface of the Au/CuMgAlO_x catalyst, and a small amount of aggregation of the Au species exists. This result is consistent with the larger average particle size of Au nanoparticles obtained from the TEM analysis. Interestingly, we find that the distribution of the Au species is similar to the dispersion trajectory of the Cu species, a phenomenon that the presence of solid electron transfer between the Au and Cu species may cause.

**Figure 13.** TEM micrographs of the Au/CuMgAlO_x catalyst, and the corresponding elemental mappings.

We have tried to describe the reaction mechanism of the Au/MgAl₂O₄ catalyst in the C₂H₂ selective hydrogenation reaction. The interface between the Au and copper species would be the active site, and Scheme 1 illustrates a possible mechanism. Introducing the Cu species increased the proportion of Au^{δ+} in the catalyst and enhanced the C₂H₂ adsorption capacity. The partially positively charged Au present at the Au-Cu interface was the site for the adsorption activation of H₂ molecules, and a small portion of H₂ molecules were adsorbed and activated on the surface of the Cu species. The hydrogen overflow between Au and Cu facilitated the hydrogenation of acetylene, which improved the catalytic performance. C₂H₄ is more readily desorbed from the Au surface than C₂H₂, making it difficult for the reduced C₂H₂ molecules to over-hydrogenate into other by-products.



Scheme 1. The preparation processes and the possible catalytic mechanism of Au/CuMgAlO_x.

3. Materials and Methods

3.1. Catalyst Preparation

MMgAlO_x (M:Mg:Al = 5:45:50 metal oxide molar ratio) mixed oxide supports were prepared by the co-precipitation method from metal salt solutions. All the materials used were of analytical purity. In a typical procedure, to prepare the CoMgAlO_x support, the desired amount of metal precursor was dissolved in double-distilled water and mixed under mild stirring conditions (Solution A). After the dropwise addition of liquid A was completed, the stirring was continued in a water bath for 12 h. The filtrate was pumped and washed until the filtrate was neutral, and the filter cake was dried in a drying oven for 12 h, ground, and then the powder was roasted in a muffle furnace at 500 °C (5 °C/min) for 4 h to obtain the CoMgAlO_x support. Similarly, CuMgAlO_x, NiMgAlO_x, and MgAl₂O₄ were prepared under the same conditions and by the same method. Au was loaded by a modified deposition–precipitation method [28]. First, the amount of chloroauric acid solution required was calculated based on the amount of Au loaded. Subsequently, the required chloroauric acid solution was pipetted into a beaker with a pipette gun, an appropriate amount of deionized water (depending on the amount of water absorbed by the support) was added, shaken well, and then the pH of the mixture was adjusted to 7–8 with KOH (1.0 M). The support was added to the above solution and ultrasonically dispersed homogeneously. It was left to stand for 4 h, poured into dilute ammonia to soak and treat for 24 h, filtered and washed until the presence of Cl[−] could not be detected, and then dried in an oven at 60 °C for 12 h to obtain the Au/MMgAlO_x catalyst. For comparison, Au/MgAl₂O₄ samples were also synthesized under the same conditions. ICP measurements showed that the corresponding Au loadings for Au/MMgAlO_x (Cu, Co, and Ni) were 0.38, 0.46, and 0.51 wt.%, respectively, and that those of Au/CuMgAlO_x were lower than those of the Au/MgAl₂O₄ catalyst (0.42 wt.%).

3.2. Catalyst Characterization

X-ray powder diffraction (XRD): Tests were carried out on a Shimadzu (Kyoto, Japan) XRD-6100 X-ray diffractometer using a Cu K α diffractive light source with a wavelength of 1.54 Å, an operating voltage of 40 kV, an operating current of 100 mA, a test range of 5 to 80°, and a scanning speed of 20°/min. Nitrogen physical adsorption and desorption

(BET): The samples were physically adsorbed and desorbed in nitrogen using an ASAP 2020 analyzer (Micromeritics, Norcross, GA, USA). The samples were first degassed under vacuum at 200 °C, and then tested in liquid nitrogen for adsorption and desorption. The test results were calculated using the BET method to obtain the samples' specific surface area, and the samples' pore size distribution was obtained using the BJH method.

Inductively coupled plasma emission spectrometry (ICP-OES): The samples were weighed and treated with freshly prepared aqua regia for 24 h. All samples were then transferred to volumetric flasks and filtered to obtain a clear solution, which was tested for the actual content of the elements in the samples on a PE optima 8000 instrument (Waltham, MA, USA). Scanning electron microscope (SEM): The catalyst morphology was observed on a JSM-7900F (JEOL, Akishima, Tokyo, Japan) scanning electron microscope. High-resolution transmission electron microscopy (TEM): TEM images of the samples were taken on an FEI (Lausanne, Switzerland) TF20 transmission electron microscope with the energy spectrum model Super-X.

NH₃ programmed temperature rise desorption (NH₃-TPD): This was carried out on a TP-5080 fully automated multiple adsorption instrument. After the support gas flow (He gas stream, 30 mL/min) was stabilized, the sample was pretreated at 250 °C for 2 h. When the temperature was lowered to 50 °C, the sample was switched to 10% NH₃/He adsorption for 30 min, followed by blowing the He gas stream. After the baseline was stabilized, the test was carried out in the range of 50~800 °C at a heating rate of 10 °C/min, and a TCD detector detected the recordings. CO₂ programmed thermal desorption (CO₂-TPD): similar to NH₃-TPD, but the test gas was changed to CO₂.

X-ray photoelectron spectroscopy (XPS): The XPS was conducted using a Thermo-Fisher Escalab 250Xi electron spectrometer (Waltham, MA, USA) with Al Ka (1486.6 eV). The surface elemental composition and chemical valence states of the Au/MMgAlO_x (M=Cu, Co, and Ni) catalysts were measured using X-ray photoelectron spectroscopy (XPS) with a Thermo-Fisher Escalab 250Xi electron spectrometer (Waltham, MA, USA). The spectrum excitation energy was set at 20 eV. The results were corrected using the C 1s peak with a binding energy of 284.8 eV. Spectral analysis was conducted using CasaXPS (Casa2318PR1-0) software, and the W Tougaard background type was selected for fitting the XPS curves.

3.3. Catalytic Activity Measurement

The catalytic performance of acetylene selective hydrogenation was tested by loading 0.1 g of catalyst into a U-shaped quartz tube reactor at a temperature of 100~350 °C, with a test interval of 50 °C and an injection interval of 25 min. The gas composition was 0.6% C₂H₂ + 3.0% H₂ + 96.4% Ar (*v/v*), and the reaction airspeed was 17,200 mL·g_{cat}⁻¹·h⁻¹. The gas composition was analyzed online by Shimadzu GC-2014 gas chromatography (FID (HP-ALUMINA), TCD). Based on the analytical results, the acetylene conversion (X) and ethylene selectivity (S) were calculated using the following equations:

$$X = \frac{(C_2H_2)_{in} - (C_2H_2)_{out}}{(C_2H_2)_{in}} \times 100\% \quad (1)$$

$$S = \frac{(C_2H_4)_{out}}{(C_2H_2)_{in} - (C_2H_2)_{out}} \times 100\% \quad (2)$$

where (C₂H₂)_{in}, (C₂H₂)_{out}, and (C₂H₄)_{out} are the concentrations of inlet acetylene, outlet acetylene, and outlet ethylene, respectively.

We evaluated the activity of the catalyst in terms of turnover rates (TORs) [76]:

$$TORs = A/B$$

$$A = V_{[C_2H_2]} \times X$$

$$B = V_m \times m_{[Au]}$$

where V_[C₂H₂] is the flow rate of acetylene, X is acetylene conversion, V_m is the molar volume of gas, and m_[Au] is actual loading of Au.

4. Conclusions

This study demonstrates that the Au/CuMgAlO_x catalyst has a superior catalytic performance to Au/MMgAlO_x (M=Ni/Co) and Au/MgAl₂O₄. The catalytic activity of its CuMgAlO_x support demonstrates that the Au component plays a significant role in the C₂H₂ reduction reaction. At lower temperatures (250 °C), the Au/CuMgAlO_x catalyst exhibits nearly 100% selectivity towards C₂H₄ and achieves a conversion rate of up to 38% for C₂H₂, with a TOR value of 0.0598 h⁻¹. However, the TOR of Au/MgAl₂O₄ is only 0.0016 h⁻¹ at 250 °C. The introduction of dopants effectively enhances the catalytic activity and stability of the Au catalyst. The BET results indicate that the Au/CuMgAlO_x catalyst possesses a large specific surface area and excellent pore properties, which are important reasons for its high catalytic activity. According to the results of CO₂-TPD and NH₃-TPD, the introduction of the dopant significantly alters the acid–base sites of the parent support. The Au/CuMgAlO_x catalysts have a high base-to-acid ratio. The XPS results show that some of the Au NPs on the surface of the Au/CuMgAlO_x catalyst are deficient in electrons. Based on the XPS results of CuMgAlO_x, we believe that there might be a strong electronic synergy between Au and Cu. Introducing dopants reduces the electron density of some Au species and changes the acidity of the support. The catalyst stability is improved by enhancing the catalytic activity and inhibiting the formation of many "hard" carbon deposits. Valuable information for the rational design of Au-based catalysts for the selective hydrogenation of acetylene can be gleaned from these results.

Author Contributions: Conceptualization, C.Q. and X.S.; methodology, X.S. and C.Q.; formal analysis, X.S., C.Q., W.L. and Y.C.; investigation, X.S., C.Q., Z.W., L.Z., H.S. and L.S.; resources, X.S. and C.Q.; writing—original draft preparation, X.S., W.L., Y.C. and C.Q.; writing—review and editing, C.Q., Z.W., X.S., W.L. and L.S.; supervision, X.S. and C.Q.; project administration, X.S. and C.Q.; funding acquisition, X.S. and Z.W. All authors have read and agreed to the published version of the manuscript.

Funding: The authors are grateful for financial support from the Shandong Natural Science Foundation (ZR 2022MB082, ZR 2022QB120), the Natural Science Foundation of Gansu Province (No. 23JRRA718), the National Natural Science Foundation of China (21603181, 21802117), and the Science and Technology Innovation Development Plan of Yantai (2023JCYJ075).

Data Availability Statement: The data presented in this study are available on request from the corresponding author via e-mail: qicx@ytu.edu.cn (C.Q.), zifanwang0316@gmail.com (Z.W.).

Acknowledgments: Thank you for the sample characterization equipment provided by the sample testing platform of Yantai University.

Conflicts of Interest: The authors declare no conflicts of interest.

References

1. Ngamsom, B.; Bogdanchikova, N.; Avalos Borja, M.; Praserttham, P. Characterisations of Pd–Ag/Al₂O₃ catalysts for selective acetylene hydrogenation: Effect of pretreatment with NO and N₂O. *Catal. Commun.* **2004**, *5*, 243–248. [[CrossRef](#)]
2. Borodziński, A.; Bond, G.C. Selective Hydrogenation of Ethyne in Ethene-Rich Streams on Palladium Catalysts. Part 1. Effect of Changes to the Catalyst During Reaction. *Catal. Rev.* **2006**, *48*, 91–144. [[CrossRef](#)]
3. Liu, X.; Li, Y.; Lee, J.W.; Hong, C.-Y.; Mou, C.-Y.; Jang, B.W.L. Selective hydrogenation of acetylene in excess ethylene over SiO₂ supported Au–Ag bimetallic catalyst. *Appl. Catal. A Gen.* **2012**, *439–440*, 8–14. [[CrossRef](#)]
4. Somorjai, G.A.; Park, J.Y. Molecular Factors of Catalytic Selectivity. *Angew. Chem. Int. Ed.* **2008**, *47*, 9212–9228. [[CrossRef](#)] [[PubMed](#)]
5. Benavidez, A.D.; Burton, P.D.; Nogales, J.L.; Jenkins, A.R.; Ivanov, S.A.; Miller, J.T.; Karim, A.M.; Datye, A.K. Improved selectivity of carbon-supported palladium catalysts for the hydrogenation of acetylene in excess ethylene. *Appl. Catal. A Gen.* **2014**, *482*, 108–115. [[CrossRef](#)]
6. Chen, Y.; Chen, J. Selective hydrogenation of acetylene on SiO₂ supported Ni–In bimetallic catalysts: Promotional effect of In. *Appl. Surf. Sci.* **2016**, *387*, 16–27. [[CrossRef](#)]
7. Yang, B.; Burch, R.; Hardacre, C.; Headdock, G.; Hu, P. Origin of the Increase of Activity and Selectivity of Nickel Doped by Au, Ag, and Cu for Acetylene Hydrogenation. *ACS Catal.* **2012**, *2*, 1027–1032. [[CrossRef](#)]

8. Zhang, Z.; Peh, S.B.; Wang, Y.; Kang, C.; Fan, W.; Zhao, D. Efficient Trapping of Trace Acetylene from Ethylene in an Ultramicroporous Metal–Organic Framework: Synergistic Effect of High-Density Open Metal and Electronegative Sites. *Angew. Chem. Int. Ed.* **2020**, *59*, 18927–18932. [[CrossRef](#)]
9. McEwan, L.; Julius, M.; Roberts, S.; Fletcher, J.C.Q. A review of the use of gold catalysts in selective hydrogenation reactions. *Gold Bull.* **2010**, *43*, 298–306.
10. McCue, A.J.; Anderson, J.A. Recent advances in selective acetylene hydrogenation using palladium containing catalysts. *Front. Chem. Sci. Eng.* **2015**, *9*, 142–153. [[CrossRef](#)]
11. McCue, A.J.; Guerrero-Ruiz, A.; Ramirez-Barria, C.; Rodríguez-Ramos, I.; Anderson, J.A. Selective hydrogenation of mixed alkyne/alkene streams at elevated pressure over a palladium sulfide catalyst. *J. Catal.* **2017**, *355*, 40–52. [[CrossRef](#)]
12. Borodziński, A.; Bond, G.C. Selective Hydrogenation of Ethyne in Ethene-Rich Streams on Palladium Catalysts, Part 2: Steady-State Kinetics and Effects of Palladium Particle Size, Carbon Monoxide, and Promoters. *Catal. Rev.* **2008**, *50*, 379–469. [[CrossRef](#)]
13. Zhang, S.; Chen, C.-Y.; Jang, B.W.L.; Zhu, A.-M. Radio-frequency H₂ plasma treatment of AuPd/TiO₂ catalyst for selective hydrogenation of acetylene in excess ethylene. *Catal. Today* **2015**, *256*, 161–169. [[CrossRef](#)]
14. Chesnokov, V.V.; Svintsitskii, D.A.; Chichkan, A.S.; Parmon, V.N. Effect of the structure of carbon support on the selectivity of Pt/C catalysts for the hydrogenation of acetylene to ethylene. *Nanotechnologies Russ.* **2018**, *13*, 246–255. [[CrossRef](#)]
15. Thomas, J.M.; Raja, R.; Lewis, D.W. Single-Site Heterogeneous Catalysts. *Angew. Chem. Int. Ed.* **2005**, *44*, 6456–6482. [[CrossRef](#)] [[PubMed](#)]
16. Shao, L.; Zhang, W.; Armbrüster, M.; Teschner, D.; Girgsdies, F.; Zhang, B.; Timpe, O.; Friedrich, M.; Schlögl, R.; Su, D.S. Nanosizing Intermetallic Compounds onto Carbon Nanotubes: Active and Selective Hydrogenation Catalysts. *Angew. Chem. Int. Ed.* **2011**, *50*, 10231–10235. [[CrossRef](#)] [[PubMed](#)]
17. Huang, D.C.; Chang, K.H.; Pong, W.F.; Tseng, P.K.; Hung, K.J.; Huang, W.F. Effect of Ag-promotion on Pd catalysts by XANES. *Catal. Lett.* **1998**, *53*, 155–159. [[CrossRef](#)]
18. Pei, G.X.; Liu, X.Y.; Yang, X.; Zhang, L.; Wang, A.; Li, L.; Wang, H.; Wang, X.; Zhang, T. Performance of Cu-Alloyed Pd Single-Atom Catalyst for Semihydrogenation of Acetylene under Simulated Front-End Conditions. *ACS Catal.* **2017**, *7*, 1491–1500. [[CrossRef](#)]
19. Zhou, H.; Yang, X.; Li, L.; Liu, X.; Huang, Y.; Pan, X.; Wang, A.; Li, J.; Zhang, T. PdZn Intermetallic Nanostructure with Pd–Zn–Pd Ensembles for Highly Active and Chemoselective Semi-Hydrogenation of Acetylene. *ACS Catal.* **2016**, *6*, 1054–1061. [[CrossRef](#)]
20. Cao, Y.; Sui, Z.; Zhu, Y.; Zhou, X.; Chen, D. Selective Hydrogenation of Acetylene over Pd-In/Al₂O₃ Catalyst: Promotional Effect of Indium and Composition-Dependent Performance. *ACS Catal.* **2017**, *7*, 7835–7846. [[CrossRef](#)]
21. Ma, C.; Du, Y.; Feng, J.; Cao, X.; Yang, J.; Li, D. Fabrication of supported PdAu nanoflower catalyst for partial hydrogenation of acetylene. *J. Catal.* **2014**, *317*, 263–271. [[CrossRef](#)]
22. Armbrüster, M.; Wowsnick, G.; Friedrich, M.; Heggen, M.; Cardoso-Gil, R. Synthesis and Catalytic Properties of Nanoparticulate Intermetallic Ga–Pd Compounds. *J. Am. Chem. Soc.* **2011**, *133*, 9112–9118. [[CrossRef](#)]
23. Menezes, W.G.; Altmann, L.; Zielasek, V.; Thiel, K.; Bäumer, M. Bimetallic Co–Pd catalysts: Study of preparation methods and their influence on the selective hydrogenation of acetylene. *J. Catal.* **2013**, *300*, 125–135. [[CrossRef](#)]
24. Han, Y.; Peng, D.; Xu, Z.; Wan, H.; Zheng, S.; Zhu, D. TiO₂ supported Pd@Ag as highly selective catalysts for hydrogenation of acetylene in excess ethylene. *Chem. Commun.* **2013**, *49*, 8350–8352. [[CrossRef](#)]
25. Huang, X.; Xia, Y.; Cao, Y.; Zheng, X.; Pan, H.; Zhu, J.; Ma, C.; Wang, H.; Li, J.; You, R.; et al. Enhancing both selectivity and coking-resistance of a single-atom Pd₁/C₃N₄ catalyst for acetylene hydrogenation. *Nano Res.* **2017**, *10*, 1302–1312. [[CrossRef](#)]
26. Ding, L.; Yi, H.; Zhang, W.; You, R.; Cao, T.; Yang, J.; Lu, J.; Huang, W. Activating Edge Sites on Pd Catalysts for Selective Hydrogenation of Acetylene via Selective Ga₂O₃ Decoration. *ACS Catal.* **2016**, *6*, 3700–3707. [[CrossRef](#)]
27. Kim, W.-J.; Moon, S.H. Modified Pd catalysts for the selective hydrogenation of acetylene. *Catal. Today* **2012**, *185*, 2–16. [[CrossRef](#)]
28. Sun, X.; Su, H.; Lin, Q.; Han, C.; Zheng, Y.; Sun, L.; Qi, C. Au/Cu–Fe–La–Al₂O₃: A highly active, selective and stable catalysts for preferential oxidation of carbon monoxide. *Appl. Catal. A Gen.* **2016**, *527*, 19–29. [[CrossRef](#)]
29. Wei, H.; Wei, X.; Yang, X.; Yin, G.; Wang, A.; Liu, X.; Huang, Y.; Zhang, T. Supported Au–Ni nano-alloy catalysts for the chemoselective hydrogenation of nitroarenes. *Chin. J. Catal.* **2015**, *36*, 160–167. [[CrossRef](#)]
30. Tan, Y.; Liu, X.Y.; Zhang, L.; Wang, A.; Li, L.; Pan, X.; Miao, S.; Haruta, M.; Wei, H.; Wang, H.; et al. ZnAl-Hydroxalite-Supported Au₂₅ Nanoclusters as Precatalysts for Chemoselective Hydrogenation of 3-Nitrostyrene. *Angew. Chem. Int. Ed.* **2017**, *56*, 2709–2713. [[CrossRef](#)]
31. Qi, C.; Huang, J.; Bao, S.; Su, H.; Akita, T.; Haruta, M. Switching of reactions between hydrogenation and epoxidation of propene over Au/Ti-based oxides in the presence of H₂ and O₂. *J. Catal.* **2011**, *281*, 12–20. [[CrossRef](#)]
32. Liu, C.; Zhang, J.; Huang, J.; Zhang, C.; Hong, F.; Zhou, Y.; Li, G.; Haruta, M. Efficient Aerobic Oxidation of Glucose to Gluconic Acid over Activated Carbon-Supported Gold Clusters. *ChemSusChem* **2017**, *10*, 1976–1980. [[CrossRef](#)]
33. Nkosi, B.; Coville, N.J.; Hutchings, G.J. Vapour Phase Hydrochlorination of Acetylene with Group VIII and IB Metal Chloride Catalysts. *Appl. Catal.* **1988**, *43*, 33–39. [[CrossRef](#)]
34. Segura, Y.; Lopez, N.; Perezramirez, J. Origin of the superior hydrogenation selectivity of gold nanoparticles in alkyne + alkene mixtures: Triple- versus double-bond activation. *J. Catal.* **2007**, *247*, 383–386. [[CrossRef](#)]
35. Gluhoi, A.C.; Bakker, J.W.; Nieuwenhuys, B.E. Gold, still a surprising catalyst: Selective hydrogenation of acetylene to ethylene over Au nanoparticles. *Catal. Today* **2010**, *154*, 13–20. [[CrossRef](#)]

36. Chai, M.; Liu, X.; Li, L.; Pei, G.; Ren, Y.; Su, Y.; Cheng, H.; Wang, A.; Zhang, T. SiO₂-supported Au-Ni bimetallic catalyst for the selective hydrogenation of acetylene. *Chin. J. Catal.* **2017**, *38*, 1338–1346. [[CrossRef](#)]
37. Zhou, H.; Li, B.; Zhang, Y.; Yan, X.; Lv, W.; Wang, X.; Yuan, B.; Liu, Y.; Yang, Z.; Lou, X. Au³⁺ Species Boost the Catalytic Performance of Au/ZnO for the Semi-hydrogenation of Acetylene. *ACS Appl. Mater. Interfaces* **2021**, *13*, 40429–40440. [[CrossRef](#)]
38. Yan, X.; Bao, J.; Yuan, C.; Wheeler, J.; Lin, W.-Y.; Li, R.; Jang, B.W.L. Gold on carbon and titanium oxides composites: Highly efficient and stable acetylene hydrogenation in large excess of ethylene. *J. Catal.* **2016**, *344*, 194–201. [[CrossRef](#)]
39. Jia, J.F.; Kenta, H.; Junko, N.K.; Kazunari, D.; Kenzi, T. Selective Hydrogenation of Acetylene over Au/Al₂O₃ Catalyst. *J. Phys. Chem. B* **2000**, *104*, 11153–11156. [[CrossRef](#)]
40. Chai, M.Q.; Tan, Y.; Pei, G.X.; Li, L.; Zhang, L.; Liu, X.Y.; Wang, A.; Zhang, T. Crystal Plane Effect of ZnO on the Catalytic Activity of Gold Nanoparticles for the Acetylene Hydrogenation Reaction. *J. Phys. Chem. C* **2017**, *121*, 19727–19734.
41. Liu, X.; Mou, C.-Y.; Lee, S.; Li, Y.; Secret, J.; Jang, B.W.L. Room temperature O₂ plasma treatment of SiO₂ supported Au catalysts for selective hydrogenation of acetylene in the presence of large excess of ethylene. *J. Catal.* **2012**, *285*, 152–159. [[CrossRef](#)]
42. Zhang, X.; Shi, H.; Xu, B.Q. Catalysis by Gold: Isolated Surface Au³⁺ Ions are Active Sites for Selective Hydrogenation of 1,3-Butadiene over Au/ZrO₂ Catalysts. *Angew. Chem. Int. Ed.* **2005**, *44*, 7132–7135. [[CrossRef](#)]
43. Fujitani, T.; Nakamura, I.; Akita, T.; Okumura, M.; Haruta, M. Hydrogen Dissociation by Gold Clusters. *Angew. Chem. Int. Ed.* **2009**, *48*, 9515–9518. [[CrossRef](#)] [[PubMed](#)]
44. Li, Z.; Li, Y.; Li, J. Support effects on the dissociation of hydrogen over gold clusters on ZnO(101) surface: Theoretical insights. *J. Chem. Phys.* **2012**, *137*, 234704. [[CrossRef](#)] [[PubMed](#)]
45. Qi, C.; Zhu, S.; Su, H.; Lin, H.; Guan, R. Stability improvement of Au/Fe-La-Al₂O₃ catalyst via incorporating with a Fe_xO_y layer in CO oxidation process. *Appl. Catal. B Environ.* **2013**, *138–139*, 104–112. [[CrossRef](#)]
46. Nikolaev, S.A.; Smirnov, V.V. Synergistic and size effects in selective hydrogenation of alkynes on gold nanocomposites. *Catal. Today* **2009**, *147*, S336–S341. [[CrossRef](#)]
47. Yan, X.; Wheeler, J.; Jang, B.; Lin, W.-Y.; Zhao, B. Stable Au catalysts for selective hydrogenation of acetylene in ethylene. *Appl. Catal. A Gen.* **2014**, *487*, 36–44. [[CrossRef](#)]
48. Azizi, Y.; Petit, C.; Pitchon, V. Formation of polymer-grade ethylene by selective hydrogenation of acetylene over Au/CeO₂ catalyst. *J. Catal.* **2008**, *256*, 338–344. [[CrossRef](#)]
49. Zhang, Y.; Sun, X.; Zhao, Y.; Su, H.; Murayama, T.; Qi, C. C, N Co-Decorated Alumina-Supported Au Nanoparticles: Enhanced Catalytic Performance for Selective Hydrogenation of Acetylene. *Top. Catal.* **2020**, *64*, 197–205. [[CrossRef](#)]
50. Sun, L.; Jiang, L.; Hua, X.; Zheng, Y.; Sun, X.; Zhang, M.; Su, H.; Qi, C. Preparation of Au/xCeO₂-Al₂O₃ catalysts with enhanced catalytic properties for the selective acetylene hydrogenation. *J. Alloys Compd.* **2019**, *811*, 152052. [[CrossRef](#)]
51. Sun, X.; Li, F.; Shi, J.; Zheng, Y.; Su, H.; Sun, L.; Peng, S.; Qi, C. Gold nanoparticles supported on MgO_x-Al₂O₃ composite oxide: An efficient catalyst for selective hydrogenation of acetylene. *Appl. Surf. Sci.* **2019**, *487*, 625–633. [[CrossRef](#)]
52. Peng, S.; Sun, X.; Sun, L.; Zhang, M.; Zheng, Y.; Su, H.; Qi, C. Selective Hydrogenation of Acetylene Over Gold Nanoparticles Supported on CeO₂ Pretreated Under Different Atmospheres. *Catal. Lett.* **2018**, *149*, 465–472. [[CrossRef](#)]
53. Tian, J.; Liu, H.; Li, P.; Huang, Z.; Chen, J. Selective oxidation of 1,2-propanediol to lactic acid over Cu-modified Au/hydrotalcite catalysts. *New J. Chem.* **2020**, *44*, 16311–16319. [[CrossRef](#)]
54. Benkhalif, A.; Kolli, M. Synthesis of Pure Magnesium Aluminate Spinel (MgAl₂O₄) from Waste Aluminum Dross. *Waste Biomass Valorization* **2022**, *13*, 2637–2649. [[CrossRef](#)]
55. Cavani, F.F. Trifirò, Vaccari, A. Hydrotalcite-type anionic clays: Preparation, properties and applications. *Catal. Today* **1991**, *11*, 173–301. [[CrossRef](#)]
56. Duan, Z.; Zhang, M.; Bian, H.; Wang, Y.; Zhu, L.; Xiang, Y.; Xia, D. Copper(II)-β-cyclodextrin and CuO functionalized graphene oxide composite for fast removal of thiophenic sulfides with high efficiency. *Carbohydr. Polym.* **2020**, *228*, 115385. [[CrossRef](#)]
57. Zhang, Y.; Cui, X.; Shi, F.; Deng, Y. Nano-Gold Catalysis in Fine Chemical Synthesis. *Chem. Rev.* **2011**, *112*, 2467–2505. [[CrossRef](#)] [[PubMed](#)]
58. Ichiji, M.; Akiba, H.; Hirasawa, I. Size Control of Au NPs Supported by PH Operation. *J. Cryst. Growth* **2017**, *469*, 168–171. [[CrossRef](#)]
59. Wan, X.; Deng, W.; Zhang, Q.; Wang, Y. Magnesia-supported gold nanoparticles as efficient catalysts for oxidative esterification of aldehydes or alcohols with methanol to methyl esters. *Catal. Today* **2014**, *233*, 147–154. [[CrossRef](#)]
60. Li, H.; Tan, Y.; Chen, X.; Yang, W.; Huang, C.; Li, J.; Ding, Y. Efficient Synthesis of Methyl Methacrylate by One Step Oxidative Esterification over Zn-Al-Mixed Oxides Supported Gold Nanocatalysts. *Catalysts* **2021**, *11*, 162. [[CrossRef](#)]
61. Ren, J.; Liu, Y.-L. Boosting syngas production from corncob tar reforming over Ni/MgAl hydrotalcite-derived catalysts. *Fuel* **2022**, *307*, 121779. [[CrossRef](#)]
62. Díez, V. Effect of the chemical composition on the catalytic performance of Mg_yAlO_x catalysts for alcohol elimination reactions. *J. Catal.* **2003**, *215*, 220–233. [[CrossRef](#)]
63. Galvita, V.; Siddiqi, G.; Sun, P.; Bell, A.T. Ethane dehydrogenation on Pt/Mg(Al)O and PtSn/Mg(Al)O catalysts. *J. Catal.* **2010**, *271*, 209–219. [[CrossRef](#)]
64. Arab, L.; Boutahala, M.; Djellouli, B.; Dintzer, T.; Pitchon, V. Characteristics of gold supported on nickel-containing hydrotalcite catalysts in CO oxidation. *Appl. Catal. A Gen.* **2014**, *475*, 446–460. [[CrossRef](#)]

65. Xia, H.; An, J.; Hong, M.; Xu, S.; Zhang, L.; Zuo, S. Aerobic oxidation of 5-hydroxymethylfurfural to 2,5-difurancarboxylic acid over Pd-Au nanoparticles supported on Mg-Al hydrotalcite. *Catal. Today* **2019**, *319*, 113–120. [[CrossRef](#)]
66. Sudarsanam, P.; Mallesham, B.; Reddy, P.S.; Großmann, D.; Grünert, W.; Reddy, B.M. Nano-Au/CeO₂ catalysts for CO oxidation: Influence of dopants (Fe, La and Zr) on the physicochemical properties and catalytic activity. *Appl. Catal. B Environ.* **2014**, *144*, 900–908. [[CrossRef](#)]
67. Chou, J.; McFarland, E.W. Direct propylene epoxidation on chemically reduced Au nanoparticles supported on titania. *Chem. Commun.* **2004**, *14*, 1468–1469.
68. Kitsudo, Y.; Iwamoto, A.; Matsumoto, H.; Mitsuhara, K.; Nishimura, T.; Takizawa, M.; Akita, T.; Maeda, Y.; Kido, Y. Final state effect for Au 4f line from gold-nano-particles grown on oxides and HOPG supports. *Surf. Sci.* **2009**, *603*, 2108–2114. [[CrossRef](#)]
69. Deng, W.; Jesus, J.D.; Saltsburg, H.; Flytzani-Stephanopoulos, M. Low-content gold-ceria catalysts for the water–gas shift and preferential CO oxidation reactions. *Appl. Catal. A Gen.* **2005**, *291*, 126–135. [[CrossRef](#)]
70. Tian, Y.; Li, Y.; Zheng, Y.; Wang, M.; Zuo, C.; Huang, H.; Yin, D.; Fu, Z.; Tan, J.; Zhou, Z. Nano-Au/MCeO_x Catalysts for the Direct Oxidative Esterification of Methylacrolein to Methyl Esters. *Ind. Eng. Chem. Res.* **2019**, *58*, 19397–19405. [[CrossRef](#)]
71. Al-Aani, H.M.S.; Trandafir, M.M.; Fechete, I.; Leonat, L.N.; Badea, M.; Negrilă, C.; Popescu, I.; Florea, M.; Marcu, I.-C. Highly Active Transition Metal-Promoted CuCeMgAlO Mixed Oxide Catalysts Obtained from Multicationic LDH Precursors for the Total Oxidation of Methane. *Catalysts* **2020**, *10*, 613. [[CrossRef](#)]
72. Hong, J.; Chu, W.; Chen, M.; Wang, X.; Zhang, T. Preparation of novel titania supported palladium catalysts for selective hydrogenation of acetylene to ethylene. *Catal. Commun.* **2007**, *8*, 593–597. [[CrossRef](#)]
73. Shen, Y.; Wu, P. Two-dimensional Raman spectroscopic study on the structural changes of a poly(3-chlorothiophene) film during the heating process. *Polymer* **2006**, *47*, 7111–7114. [[CrossRef](#)]
74. Haruta, M.; Yamada, N.; Kobayashi, T.; Iijima, S. Gold Catalysts Prepared by Coprecipitation for Low-Temperature Oxidation of Hydrogen and of Carbon Monoxide. *J. Catal.* **1989**, *115*, 301–309. [[CrossRef](#)]
75. Cameron, D.; Holliday, R.; Thompson, D. Gold's future role in fuel cell systems. *J. Power Sources* **2003**, *118*, 298–303. [[CrossRef](#)]
76. Che, L.; Guo, J.; He, Z.; Zhang, H. Evidence of rate-determining step variation along reactivity in acetylene hydrogenation: A systematic kinetic study on elementary steps, kinetically relevant(s) and active species. *J. Catal.* **2022**, *414*, 336–348. [[CrossRef](#)]

Disclaimer/Publisher's Note: The statements, opinions and data contained in all publications are solely those of the individual author(s) and contributor(s) and not of MDPI and/or the editor(s). MDPI and/or the editor(s) disclaim responsibility for any injury to people or property resulting from any ideas, methods, instructions or products referred to in the content.